An Antideceptive Jamming Method for Multistatic Synthetic Aperture Radar Based on Collaborative Localization and Spatial Suppression

Wenjing Wang, *Student Member, IEEE*, Junjie Wu [ID], *Member, IEEE*, Jifang Pei [ID], *Member, IEEE*, Xinyu Mao, and Jianyu Yang [ID], *Member, IEEE*

Abstract—In recent years, the research of multistatic synthetic aperture radar (SAR) has become a hot spot because of its great potentials in military and civil applications. However, it is inevitably disturbed by electronic countermeasures. In the multistatic SAR image, the false target caused by transmitting deceptive jamming leads to misjudgment of the image information. In this article, a new antideceptive jamming method for multistatic SAR is proposed. This method can locate the deceptive jammer and effectively suppress it. First of all, the echo model of multistatic SAR in the jamming environment is set up. Based on this model, the relationship expression for the location of jammer is derived. Then, we use the maximally stable extremal region method and the Euclidean-distance-based method to detect and identify false target in the multistatic SAR image. By using the location information of false target, receivers, and transmitters, the expression of the jammer localization is solved to locate the jammer. Finally, the minimum variance distortionless response beamforming method and image mosaic method are used to effectively suppress the jamming. The simulation results show that the method is effective.

Index Terms—Antideceptive jamming, image mosaic method, jammer localization, multistatic, synthetic aperture radar (SAR), target detection.

I. Introduction

SYNTHETIC aperture radar (SAR), due to its all-day and all-weather highresolution imaging, has attracted considerable attentions [1]. It can reliably, continuously, and globally observe the dynamic changes of the earth's surface. With the development of application requirements, SAR has gradually developed from traditional SAR configuration to bistatic configuration [2]–[11] or even multistatic configuration. Among them, multistatic SAR has the advantages of flexible configuration and information acquisition from multiview, which is beneficial to

target detection, target recognition, electronic countermeasures, etc.

Compared with bistatic SAR, the research of multistatic SAR is just beginning. In multistatic SAR, different receivers image from different angles, which can provide observation information from various angles in the imaging area, and achieve application by analyzing the information. In terms of imaging, some scholars have studied the imaging scene of multistatic SAR [12], and some scholars have proposed an imaging algorithm based on fast Fourier transform for multistatic SAR [13]. In the aspect of configuration design, scholars have studied how to use the transformation of geometric configuration to realize image reconstruction [14] and topology design of spaceborne-airborne multistatic SAR [15]. More papers have done research on the application scenarios and experiments of multistatic SAR. The swarm UAV is a typical multistatic application scenario. In a variety of application scenarios, multistatic SAR can realize three-dimensional reconstruction of SAR image [16], detection, and location of mines [17], and so on by its own system advantages.

Because of its great potentials in military and civil applications, it will inevitably be subject to electronic jamming in the future battlefield. Although multistatic SAR has the advantages of flexible configuration and multidimensional information, it is still possible to be jammed. The jamming approaches to SAR are mainly divided into two categories: barrage jamming and deceptive jamming. Barrage jamming makes the real signal submerged in the jamming signal by producing similar noise jamming signal. Since jamming signal needs to achieve a certain transmission power to obtain effective jamming, it will have obvious imaging characteristics in the image, which makes it difficult to hide. Some new barrage jamming methods and correlation functions for SAR have been proposed [18], [19]. In [18], the author proposes a method of barrage noise jamming based on dual jammer, which, by changing the geometric model of jammer, can conduct jamming to moving target detection of three channel SAR. This method will cause the whole SAR image to be covered by jamming signal, so it cannot use displaced phase center antenna to detect the moving target effectively. The jamming signal ratio (J/S) function is proposed in [19], which simplifies the formula of irradiation area by using the principle of barrage jamming, and renders the realization of jamming easier. In the case of multistatic SAR, it is not feasible of hardware

power to realize jamming in multiple receivers at the same time through barrage jamming. So, in the current electronic countermeasures, the research of deceptive jamming is more extensive for multistatic SAR.

The deceptive jamming of SAR is realized through obtaining the transmitting signal of the transmitter, analyzing the relevant parameters of the transmitting signal, and finally through parameter modulation, retransmitting the jamming signal to get false target appear in the SAR image, which is difficult to be eliminated by existing antijamming methods. At present, many scholars have begun to study deceptive jamming methods of multistatic SAR. In [20], different from the way of traditional jamming signal, which is directly transmitted to the receiver, the false target generated by the jamming signal covers the target area that needs to be protected to prevent being imaged by radar. In [21], a deceptive jamming method is proposed by processing the parameters of enemy SAR based on multiple receivers. In [22], the author improves the performance of the cooperative deceptive jamming system by designing the optimal configuration of the receiver. Compared with barrage jamming, deceptive jamming consumes less power, and the jammer is more hidden [23]–[25].

Deceptive jamming mainly includes generative deceptive jamming and transmitting deceptive jamming. To generate deceptive jamming, we need to master almost all the signal parameters of the enemy radar system, and then generate jamming signals according to these signal parameters. This jamming mode requires too much investigation, and thus is not widely used at present. The transmitting deceptive jamming first receives the transmitting signal from the transmitter, and then retransmits it after some processing. Therefore, for the research of multistatic SAR jamming methods, the current scholars have more research on transmitting deceptive jamming.

With the development of transmitting deceptive jamming technology, the research of antitransmitting deceptive jamming has attracted more and more attention. At present, there are researches on related technologies under a variety of SAR. For example, in single channel SAR, antijamming technology is realized by analyzing the difference between real echo and false echo [26]. In multichannel SAR, a method of antitransmitting deceptive jamming is proposed to improve the image quality [27]. In [28], the author analyzes the antijamming methods for multichannel SAR and multiple-input multiple-output SAR. And some antideceptive jamming methods based on SAR interferometric phase have been proposed and performed very well [29]–[31]. For other SAR systems, in [32] and [33], the antideceptive jamming is realized by phase coded signal modulates the linear format modulated (LFM-PC) and orthogonal frequency division multiplexing transmission. However, in the existing research, there are few research on the antitransmitting deceptive jamming for multistatic SAR. When multistatic SAR is subjected to transmitting deceptive jamming, false targets are appeared in the image, which can make interpretation of image harder. Although there is the possibility of jamming in the multistatic SAR, the multistatic SAR can use the advantages of its multiple platform to achieve jamming suppression.

In this article, a new antideceptive jamming method for multistatic SAR is proposed. First of all, we establish the echo model of multistatic SAR in jamming environment, and deduce the relationship among jammer, receiver, and transmitter. Then, the maximally stable extremal region (MSER) algorithm and the distinguish method based on Euclidean distance are used to detect and identify false targets. Next, the location information of the false target and the configuration information of the multistatic SAR is used to locate the jammer. Finally, we use the minimum variance distortionless response (MVDR) beamforming method and image mosaic method to suppress deceptive jamming.

The follow-up structure of this article is as follows. In Section II, the echo model of multistatic SAR in jamming environment is established, and the expression for echo signal of the receiver in jamming environment is described. Section III gives the antideceptive jamming method, which mainly includes the detection and identification of false targets, the jammer localization, MVDR algorithm, and image mosaic method. In Section IV, we verify the effectiveness of the proposed method through simulation experiments. Finally, in Section V, we briefly summarize this article.

II. ECHO MODEL OF MULTISTATIC SAR IN JAMMING ENVIRONMENT

In the actual multistatic SAR, it can include multiple transmitters and multiple receivers. In this article, we mainly discuss the multistatic SAR with one transmitter and four receivers. Fig. 1(a) shows the geometric configuration of multistatic SAR in the context of transmitting deceptive jamming, and Fig. 1(b) shows the top view of the configuration. Their beam centers point at the scene center O.

The transmitting signal of transmitter is linear frequency modulated (LFM). The point target echo received by the ith receiver is as follows:

$$s(\tau, \eta; i) = A_0 w_r\left(\tau - \frac{R(\eta; i)}{c}\right) w_a(\eta - \eta_c)$$
$$\times \exp\left\{\frac{-j2\pi f_0 R(\eta; i)}{c}\right\}$$
$$\times \exp\left\{j\pi K_r\left(\tau - \frac{R(\eta; i)}{c}\right)^2\right\} \quad (1)$$

where τ represents the range time, η is the azimuth time, w_r and w_a denote the range envelope function and azimuth envelope function, respectively. η_c is the beam center crossing time, K_r represents the FM rate, c is the speed of light, and f_0 means carrier frequency. A_0 denotes the radar cross section.

The range history is the sum of the range from the transmitter to the target and the range from ith receiver to the target at the η time. $R(\eta; i)$ is the range history sum from the target to ith receiver and transmitter, whose expression is shown as follows:

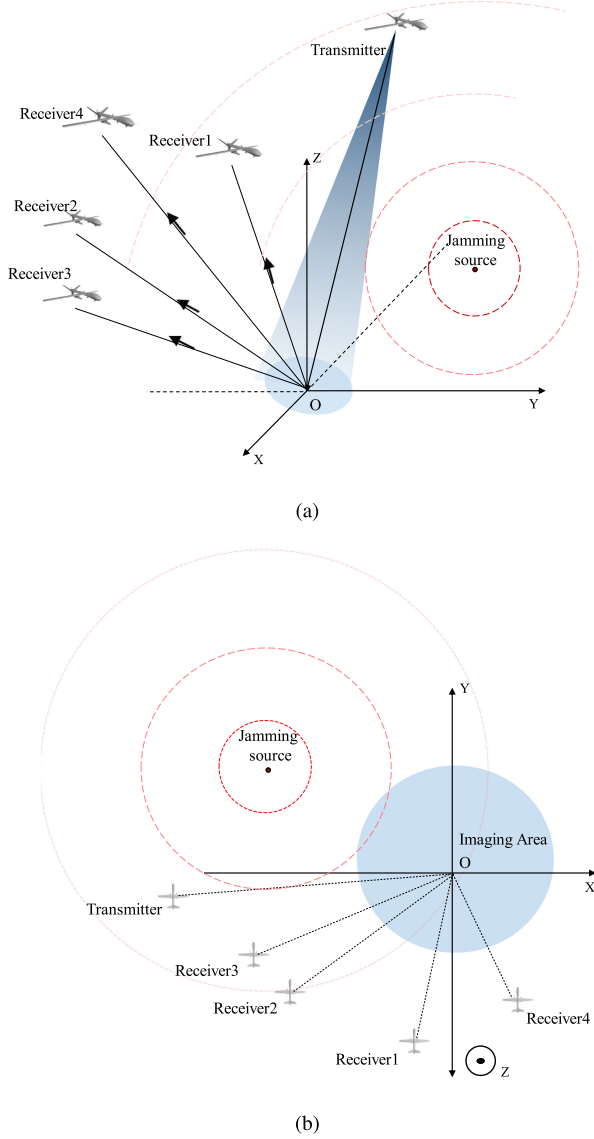$$R(\eta; i) = R_R(\eta; i) + R_T(\eta) \quad (2)$$

Fig. 1. Geometric configuration of multistatic SAR. (a) 3-D configuration graph. (b) Top view of geometry.

where $R_R(\eta; i)$ and the $R_T(\eta)$ mean the range from the target (x_p, y_p, z_p) to the ith receiver and the transmitter, respectively. And they are given as follows:

$$R_R(\eta; i)$$
$$= \sqrt{[x_i(\eta) - x_p]^2 + [y_i(\eta) - y_p]^2 + [z_i(\eta) - z_p]^2} \quad (3)$$

$$R_T(\eta)$$
$$= \sqrt{[x_T(\eta) - x_p]^2 + [y_T(\eta) - y_p]^2 + [z_T(\eta) - z_p]^2} \quad (4)$$

where (x_i, y_i, z_i), $i = 1, 2, 3, 4$ represent the location of the ith receiver. (x_T, y_T, z_T) mean the location of the transmitter.

Through parameter modulation, the transmitting deceptive jammer transmits the jamming signal after a fixed time delay. Because the jammer transmits the jamming signal, the echo

arriving at the ith receiver is shown as follows:

$$s_J(\tau, \eta; i) = A_0 w_r \left(\tau - \frac{R_J(\eta; i)}{c} - \tau_0 \right) w_a(\eta - \eta_c)$$

$$\times \exp \left\{ \frac{-j2\pi f_0 R_J(\eta; i)}{c} \right\}$$

$$\times \exp \left\{ j\pi K_r \left(\tau - \frac{R_J(\eta; i)}{c} - \tau_0 \right)^2 \right\} \quad (5)$$

where τ_0 is the fixed delay, and $R_J(\eta; i)$ is the range history sum from jammer to the ith receiver and transmitter, it can be represented as follows:

$$R_J(\eta; i) = R_{J\_R}(\eta; i) + R_{J\_T}(\eta). \quad (6)$$

The range history of the transmitter and the ith receiver to the jammer can be represented as follows:

$$R_{J\_R}(\eta; i)$$
$$= \sqrt{[x_i(\eta) - x_J]^2 + [y_i(\eta) - y_J]^2 + [z_i(\eta) - z_J]^2} \quad (7)$$

$$R_{J\_T}(\eta)$$
$$= \sqrt{[x_T(\eta) - x_J]^2 + [y_T(\eta) - y_J]^2 + [z_T(\eta) - z_J]^2} \quad (8)$$

where (x_J, y_J, z_J) are the location of the jammer.

When the receiver receives the jamming signal from the jammer, there will be false targets in the image, which will seriously affect the imaging performance of the multistatic SAR.

III. ANTIDECEPTIVE JAMMING METHOD

For the four receivers, the delay time of the jamming signal transmitted by the jammer is the same, so the displacement of the false target in the slant plane of the four receivers is the same. However, in the multistatic SAR, the relative positions between the four receivers and the transmitter are different, so the corresponding group-range plane is different. Therefore, the positions of false targets in four SAR images are different. If the location of the false target can be detected in these SAR images, the jammer can be located by combining the configuration information of the multistatic SAR. Finally, the deceptive jamming suppression is realized by using MVDR beamforming method and image mosaic method. The flowchart of the method proposed in this article is shown in Fig. 2.

A. Detection and Distinguish of False Targets

The high-value targets in the multistatic SAR image are often man-made targets, which are easy to produce strong scattering and show a stable scattering area in SAR image. At the same time, the jamming technology in recent years makes the similarity between false targets and real targets very high. Therefore, false targets and real targets both have the stable area in the image, thus MSER method is used to quickly detection the target.

In order to realize antideceptive jamming of multistatic SAR, it is necessary to detect false targets in multistatic SAR images. The MSER algorithm is an effective target detection algorithm, which has been widely used in SAR images and optical images. Compared with other detection algorithms, the MSER algorithm
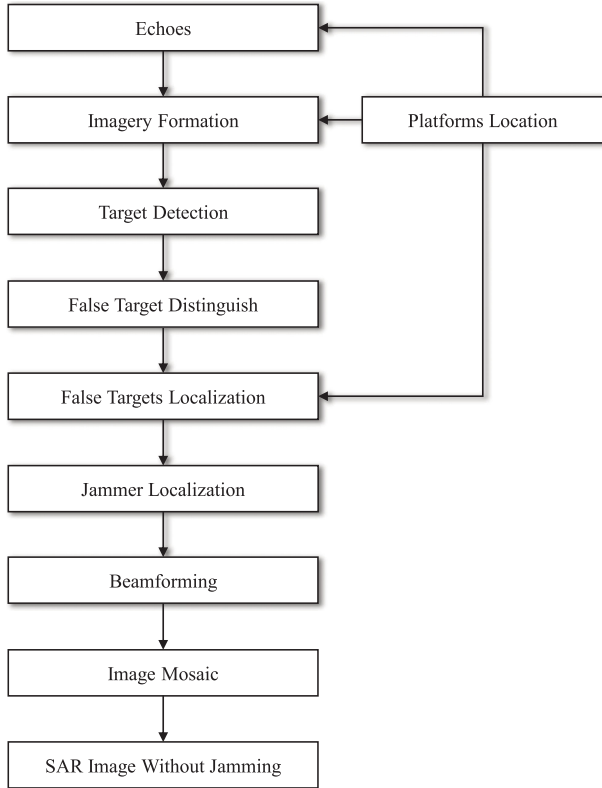
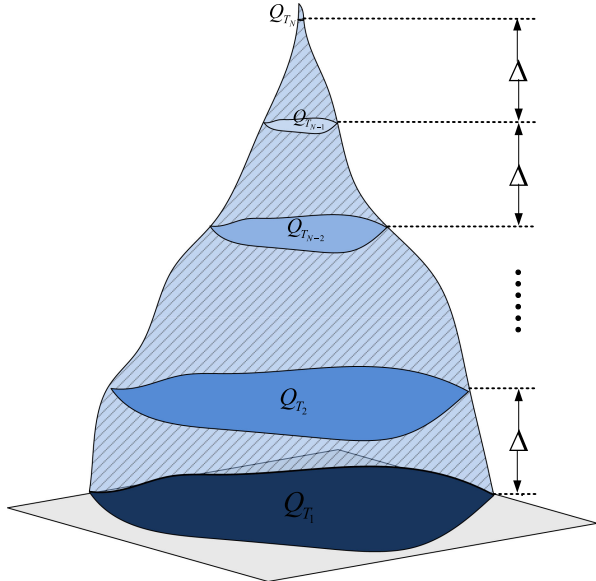Fig. 2. Flowchart of the proposed method in this article.

Fig. 3. Diagram of the MSER algorithm.

can quickly and accurately detect targets from the complex environment [34], [35]. In each image, the MSER algorithm is used to detect targets, then Euclidean distance between targets in different SAR images is calculated, and false targets in each SAR image are identified by setting a threshold.

The MSER algorithm can be divided into four steps, and the schematic diagram of MSER algorithm is shown in Fig. 3 as follows:

1) Using thresholds from 0 to 255 to binarize the image. Set the equal-interval thresholds as $\{T_i | T_{i+1} = T_i + \Delta, T_i \in [0, I], i = 1, 2, \ldots, N\}$, where $I \in [0, 255]$, Δ is the threshold interval and T_i represents the ith threshold. The gray level below the threshold is set to 0 and the gray level above the threshold is set to 1. Thus, N binary images can be obtained.

2) Utilize T_i to generate a series of mutually extreme regions, which are represented as $Q_{T_1} \supset Q_{T_2} \supset Q_{T_3} \supset \ldots \supset Q_{T_{N-1}} \supset Q_{T_N}$.

3) Set a equation as

$$q_{Ti} = \frac{\left| S(Q_{T_{i+1}}) - S(Q_{T_i}) \right|}{S(Q_{T_i})} \tag{9}$$

where $S(\cdot)$ means the area of the region, q_{T_i} represents the rate of change of area of Q_{T_1} when threshold is T_i, and ε means the upper limit of the rate of change of area.

4) Let q_{Ti} which satisfies $q_{Ti} < \varepsilon$ to form a set as H. $Q_{\text{MSER}} = \arg \min_{Q_{T_i}} H$. The MSER algorithm is selected with a stability region, and the targets in SAR images are accurately detected.

After the above steps, we use the Euclidean distance to identify false targets in multiple SAR images, and obtain location information of false targets.

First, we select two images from multiple SAR images. Let the two images be U_i and U_j, $i \neq j$, $i, j = 1, 2, 3, 4$. The false targets in the two SAR images are expressed as $\{A_j^{(m)}(x, y) | j = 1, 2, \ldots, L; m = 1, 2\}$, where $A_j^{(m)}(x, y)$ means the jth target in the mth SAR image and L is the number of jammers.

Then set β as the threshold of the Euclidean distance. And set $R_{i,j}^{(n,m)} = |A_i^{(n)}(x, y) - A_j^{(m)}(x, y)|$, where $R_{i,j}^{(n,m)}(x, y)$ represents the Euclidean distance from the ith target in the nth SAR image to the jth target in the mth SAR image. For two SAR images, the matrix B is composed by the Euclidean distance between targets, where $b_{ij} = R_{i,j}^{(1,2)}$ means the Euclidean distances from the ith target in the first SAR image to the jth target in the second SAR image. The matrix B is as follows:

$$\begin{bmatrix} R_{1,1}^{(1,2)} & R_{1,2}^{(1,2)} & \cdots & R_{1,L}^{(1,2)} \\ R_{2,1}^{(1,2)} & R_{2,2}^{(1,2)} & \cdots & R_{2,L}^{(1,2)} \\ \cdots & \cdots & \cdots & \cdots \\ R_{L,1}^{(1,2)} & R_{L,2}^{(1,2)} & \cdots & R_{L,L}^{(1,2)} \end{bmatrix} \tag{10}$$

Last, we compare b_{ij} with threshold β, when $b_{ij} > \beta$, let $b_{ij} = 1$; otherwise, $b_{ij} = 0$. If the value of ith row all are 1, it means the ith target in the first SAR image is a false target. If the values of jth column all are 1, it represents that the jth target in the second SAR image is a false target. And so on, false targets in each image can be detected and identified through the above steps.

B. Jammer Localization

Through the above steps, accurate location information of false targets in multiple SAR images are obtained. In the multistatic SAR, the position of each receiver is different. We use the relationship among false target, receiver, and transmitter to

locate the jammer. In this section, the position of the jammer can be obtained by solving its relationship with geometry configuration and false target.

In the four SAR images from different receivers, range history sum of the false target of the ith receiver is expressed as follows:

$$R_F(\eta; i) = R_{F\_T}(\eta; i) + R_{F\_R}(\eta; i) \tag{11}$$

where the $R_{F\_T}(\eta; i)$ means the range from the transmitter to the false target of the ith image, and $R_{F\_R}(\eta; i)$ means the range from the ith receiver to the false target as follows:

$$R_{F\_T}(\eta; i)$$
$$= \sqrt{[x_T(\eta) - x_{F,i}]^2 + [y_T(\eta) - y_{F,i}]^2 + [z_T(\eta) - z_{F,i}]^2} \tag{12}$$

$$R_{F\_R}(\eta; i)$$
$$= \sqrt{[x_i(\eta) - x_{F,i}]^2 + [y_i(\eta) - y_{F,i}]^2 + [z_i(\eta) - z_{F,i}]^2} \tag{13}$$

where $(x_{F,i}, y_{F,i}, z_{F,i})$, $i = 1, 2, 3, 4$ represents the location of false target in the ith image from receivers.

The range history of the false target in each SAR image can also be expressed through the location information of the jammer and the fixed time delay τ_0. The formula is as follows:

$$R_F(\eta; i) = R_{J\_T}(\eta) + R_{J\_R}(\eta; i) + c\tau_0 \tag{14}$$

where the $R_{J\_T}(\eta)$ means the range from transmitter to the jammer, and $R_{J\_R}(\eta; i)$ means the range from ith receiver to the jammer. Specific expression can be seen in (7) and (8).

According to the (11) and (14), the relationship among the configuration, the false target and the location of the jammer can be expressed. The position of the jammer can be achieved by solving (15)

$$R_{F\_T}(\eta; i) + R_{F\_R}(\eta; i) = R_{J\_T}(\eta) + R_{J\_R}(\eta; i) + c\tau_0 \tag{15}$$

In this article, the multistatic SAR is one transmitter and four receivers. The location information of receivers and the false target of each image are different, hence we can obtain four equations

$$\begin{cases} R_{F\_T}(\eta, 1) + R_{F\_R}(\eta, 1) = R_{J\_T}(\eta) + R_{J\_R}(\eta, 1) + c\tau_0 \\ R_{F\_T}(\eta, 2) + R_{F\_R}(\eta, 2) = R_{J\_T}(\eta) + R_{J\_R}(\eta, 2) + c\tau_0 \\ R_{F\_T}(\eta, 3) + R_{F\_R}(\eta, 3) = R_{J\_T}(\eta) + R_{J\_R}(\eta, 3) + c\tau_0 \\ R_{F\_T}(\eta, 4) + R_{F\_R}(\eta, 4) = R_{J\_T}(\eta) + R_{J\_R}(\eta, 4) + c\tau_0 \end{cases} \tag{16}$$

By solving the above equations, we can get the position of the jammer (x_J, y_J, z_J) and the fixed time delay τ_0. Then, we use the spatial-filtering-based beam forming and the image mosaic method to achieve the jamming suppression.

C. Jamming Signal Suppression

In order to increase flexibility of multistatic SAR, the advanced multistatic SAR is equipped with the array antennas. The digital beam formation adjusts the weighting coefficient of each array according to certain criteria, so as to ensure the beam direction, so that the radar can set the zero point in the specified direction of the antenna pattern, and suppress the jamming signal in the process. In recent years, the researches on MVDR algorithm has been more abundant, such as the application of SAR [36], [37], spatial filtering [38]–[40], and estimation of beam arrival direction [41]. The MVDR algorithm is based on the principle of maximum output signal-to-noise ratio. In this article, the MVDR algorithm is used to achieve jamming signal suppression.

Suppose there are M array elements, and L incoming signals in the space, then the received signals of the array are $y(\tau, \eta; i)$

$$\boldsymbol{y}(\tau, \eta; i) = \boldsymbol{A}\boldsymbol{x}(\tau, \eta; i) + \boldsymbol{v}(\tau, \eta; i) \tag{17}$$

where $\boldsymbol{x}(\tau, \eta; i)$ denotes the signals from the L directions and $\boldsymbol{v}(\tau, \eta; i)$ denotes noise. The matrix $\boldsymbol{A}$ includes information on the incoming signals, shown as follows:

$$\boldsymbol{A} = \begin{bmatrix} \boldsymbol{d}(\theta_0) & \boldsymbol{d}(\theta_1) & \cdots & \boldsymbol{d}(\theta_{L-1}) \end{bmatrix} \tag{18}$$

$$\boldsymbol{d}(\theta_l) = \begin{bmatrix} e^{-j\phi_{0l}} & e^{-j\phi_{1l}} & \cdots & e^{-j\phi_{(M-1)l}} \end{bmatrix}^T \tag{19}$$

where ϕ_{ml} represents the phase delay of the lth wave signal to the mth array element.

The spatial filtering of array signals gives

$$\boldsymbol{s} = \boldsymbol{\omega}^H \boldsymbol{y} \tag{20}$$

where $\boldsymbol{\omega} = [\omega_0 \ \omega_1 \ \cdots \ \omega_{M-1}]^T$ is the weighting vector of spatial filter.

The average output power P is

$$P = E\left\{|\boldsymbol{s}|^2\right\} = \boldsymbol{\omega}^H \boldsymbol{R} \boldsymbol{\omega} \tag{21}$$

where $\boldsymbol{R}$ is the spatially related matrix of the array input signal.

The MVDR algorithm obtains the optimal estimation by minimizing the output signal power. The effect of suppression or enhancement is obtained through restraining the incoming signals in different directions

$$\boldsymbol{A}^H \boldsymbol{\omega} = \boldsymbol{F} \tag{22}$$

where $\boldsymbol{F} = [f_0 \ f_1 \ \cdots \ f_{L-1}]^T$.

In order to guarantee nondistortion of the desired signal and suppress the jamming by setting zero points, the constraints are shown as follows:

$$f_0 = 1, f_i = 0 \tag{23}$$

where $i = 1, 2, 3 \cdots L-1$.

Solving constrained optimization problems

$$\min_{\boldsymbol{\omega}} \boldsymbol{\omega}^H \boldsymbol{R} \boldsymbol{\omega}$$

$$\text{s.t. } \boldsymbol{A}^H \boldsymbol{\omega} = \boldsymbol{F}. \tag{24}$$

Using the Lagrangian Submethod to construct the function

$$H(\boldsymbol{\omega}) = \frac{1}{2}\boldsymbol{\omega}^H \boldsymbol{R} \boldsymbol{\omega} + Re\left\{\boldsymbol{\lambda}^H\left(\boldsymbol{A}^H\boldsymbol{\omega} - \boldsymbol{F}\right)\right\}. \tag{25}$$

Solving the equation

$$\boldsymbol{\omega} = \boldsymbol{R}^{-1}\boldsymbol{A}(\boldsymbol{A}^H \boldsymbol{R}^{-1}\boldsymbol{A})^{-1}\boldsymbol{F}. \tag{26}$$
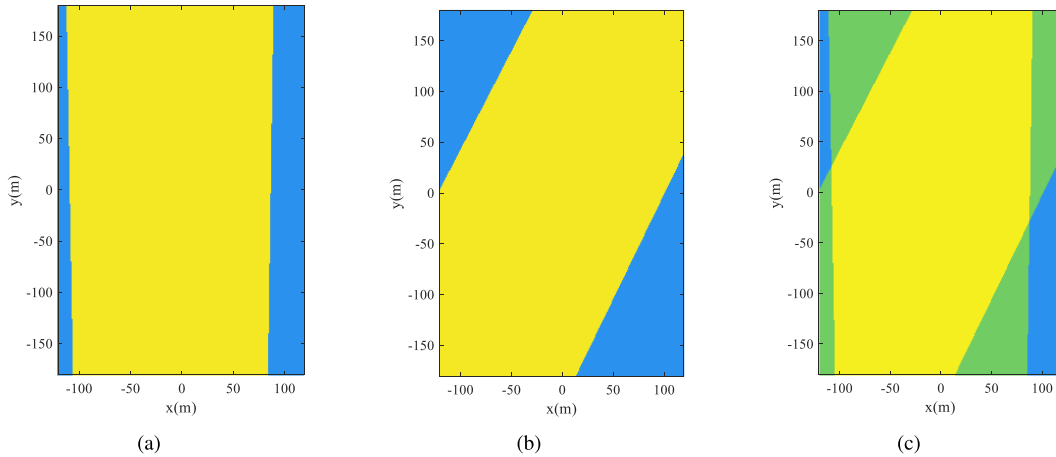
Fig. 4. Sketches of effective imaging area. (a) Sketch of effective imaging area of receiver one. (b) Sketch of effective imaging area of receiver two. (c) Sketch of effective imaging area by combining the two receivers.

D. Image Mosaic

Through the above analysis, we can know that the jamming suppression effect after beamforming is different due to the different relative positions of jammer and receivers. According to the algorithm of part III(B), the location information of the jammer can be calculated. When multistatic SAR suffers from transmitting deceptive jamming, obvious false targets are formed in SAR image. When the jammer is outside the imaging area, we use the method in part III(C) to zero the direction of the receiver to the jammer, so as to achieve jamming suppression. In SAR images, the false targets are produced by jamming signal can be effectively eliminated.

However, when the jammer is within the imaging area, if the MVDR algorithm is directly used to process, there are some areas that can not be imaged in the imaging area, which is called blind area in this article. The blind area is shown in Fig. 4(a) and (b). The blue area in the two images represents the blind area, and the yellow area represents the imageable area. In this section, we use the image mosaic method to reduce the blind area.

For the bistatic SAR, there is a large area that cannot be imaged in the SAR image, and the blind area exist around the jammer. In this article, we use the advantages of multistatic SAR, and use image mosaic method to reduce the blind area in the image domain, so as to achieve the effect of imaging area expansion. By overlapping the effective imaging area of each receiver, the imaging area is divided into many sub blocks, as shown in Fig. 4(c). These sub blocks in the imaging area may be imaged by multiple receivers at the same time. In Fig. 4(c), different colors represent different times of imaging. From the graph, we can know that the imaging times of adjacent sub blocks are different.

The best quality image of the sub block is selected in those images of the same block as follows:

$$s(k) = \sum_{i,j} \Psi\left(v_k(i,j)\right) \qquad (27)$$

where $v_k(i,j)$, is the pixel intensity on the ith row and jth column in the kth image, and the $\Psi(x)$ is a convex function. For $\Psi(x)$, there has been many different expressions. We utilize $\Psi(x) = x^2$ as the criterion for image quality judgment. Image sharpness defined by square function x^2 can describe the image focusing well when the imaging scene characteristics are unknown. Therefore, it also measures SAR imaging results widely as an important indicate [42]–[44]. The larger the value, the better the SAR image can be restored. It has been proved that the image sharpness defined by x^2 can measure the image quality effectively and reliable [45]–[47]. So, in this article, we choose $\Psi(x) = x^2$ as the standard for picture judgment.

For a sub block, (27) is used to calculate the value of the sub block in each imaging image, and set it as $s(1), s(2), \ldots, s(n)$, where the n means the number of times the sub block can be imaged. According to $s(1), s(2), \ldots, s(n)$, we can choose one of them as the best imaging quality sub block. Each sub block in the image is selected according to the above criteria. Finally, sub blocks of optimal imaging quality can be synthesized into a SAR image, which has a larger imageable area and better imaging quality than the bistatic SAR image.

IV. SIMULATION

In this section, we use a coast scene, including two ships and a coast, as the simulation scene to prove the effectiveness of the method. The simulation image is shown in Fig. 5. The center of the simulation image is the origin of the axis, the horizontal direction is the x-axis, and the vertical direction is the y-axis. The x-axis of the imaging area ranges from -240 to 240 m, the y-axis of imaging area is from -360 to 360 m. The simulation parameters are listed in the Table I.

In this article, the multistatic SAR system consists of one transmitter and four receivers. The back projection (BP) algorithm is used to imaged for the echo from each receiver. Then, we use the MSER algorithm to detect all targets. The size of minimum target in all SAR images is calculated, and half of the minimum size is selected as the threshold for the
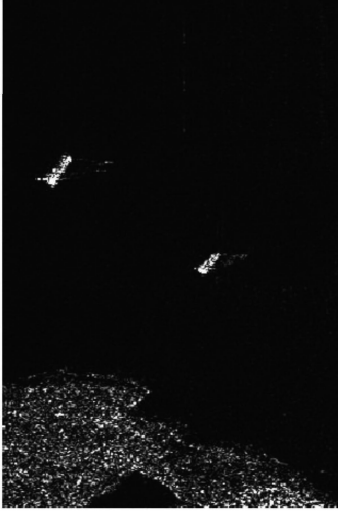
Fig. 5.   Original simulation scene.

TABLE I
SIMULATION PARAMETERS

	X	Y	Z
Transmitter	-5000m	0m	3000m
Receiver1	0m	-5000m	2200m
Receiver2	-4000m	-3000m	1600m
Receiver3	1500m	3000m	3800m
Receiver4	1000m	-500m	4600m
System Parameters			
Carrier Frequency	10GHz		
Signal Bandwidth	200MHz		
Pulse Repeating Frequency	1000Hz		
Synthetic Aperture Time	1s		

Euclidean distance. And the matrix B is established by the rule in Section III(A). The values in the matrix B is observed to determine the false target.

Here, we mainly discuss two situations. In the first situation, the jammer is outside the imaging area. we use the beamforming to achieve jamming suppression. In the other situation, the jammer is within the imaging area. We use the beamforming and image mosaic method to achieve jamming suppression.

In order to demonstrate the validity of the method proposed, we utilize the ratio of the desired signal power to interference power as certain metrics, it also called signal to interference ratio (SIR) and shown as follows:

$$\text{SIR} = 10\log_{10} \frac{\sum_{p,q} |D(x_p, y_q)|^2}{\sum_{p,q} |Y(x_p, y_q) - D(x_p, y_q)|^2} \quad (28)$$

where $D(\cdot)$ denotes the scattering coefficient from image in the presence of just the signal and $Y(\cdot)$ means the scattering coefficient from image after processing.

TABLE II
QUANTITATIVE RESULTS FOR RETRANSMITTING DECEPTIVE JAMMING
SUPPRESSION FOR SIMULATION EXPERIMENT I

SIR_1[1]	SIR_2[2]	SIR promotion
10	22.1297	12.1297
0	22.1285	22.1285
-10	22.1137	32.1137

[1] The SIR ratio before processing.
[2] The SIR ratio after processing.

In both of these two situations, we use the method proposed in this article to achieve antideceptive jamming. Simulation results can prove the effectiveness of this method.

A. Simulation Experiment I

The location of the jammer is assumed to be $(-300$ m, 150 m, 50 m), the fixed time delay is 1 μs. Fig. 6(a)–(d) is the images of four receivers in the jamming environment. From the four images, we can see that there are three ships in each image. Through the MSER algorithm and Euclidean-distance-based distinguish method, and according to the relationship between the receiver and the false target, we can identify the false target and get the location information of the false targets in the four images. In the image, the real target is in the red rectangle, and the false target is in the yellow rectangle.

Then, the beamforming is carried out for each receiver. Fig. 6(e)–(h) are the imaging results of four receivers after the MVDR algorithm, corresponding to Fig. 6 (a)–(d), respectively. In order to better observe the simulation results, Fig. 6(i) and (j) is the enlarge version of Fig. 6(a) and (e), respectively. In Fig. 6(j), the false targets in the yellow rectangle are eliminated completely. Through the method proposed in this article, only the real targets are left in the image, and the imaging performance of the real targets is not affected by beamforming.

The quantitative results for retransmitting deceptive jamming suppression for simulation experiment I are shown in Table II. Each table contains three experiments, and the first column represents the initial SIR, the second column means the SIR after processing. Each row of Table II means the result of an experiment, and the initial SIR of each experiment is different. From Table II, we can obtain the SAR image with high SIR when the power of jamming signal changing. It can be seen from above that the method proposed in this article can effectively suppress transmitting deceptive jamming, thus improving the interpretation of the picture.

In simulation experiment I, the jammer is outside the imaging area, and the false target can be effectively removed by the MVDR algorithm. After the MVDR algorithm, we can get the real SAR image without the jamming signal.

B. Simulation Experiment II

In this simulation experiment, the jammer is within the imaging area. It is assumed that the location of the jammer is $(-180,$
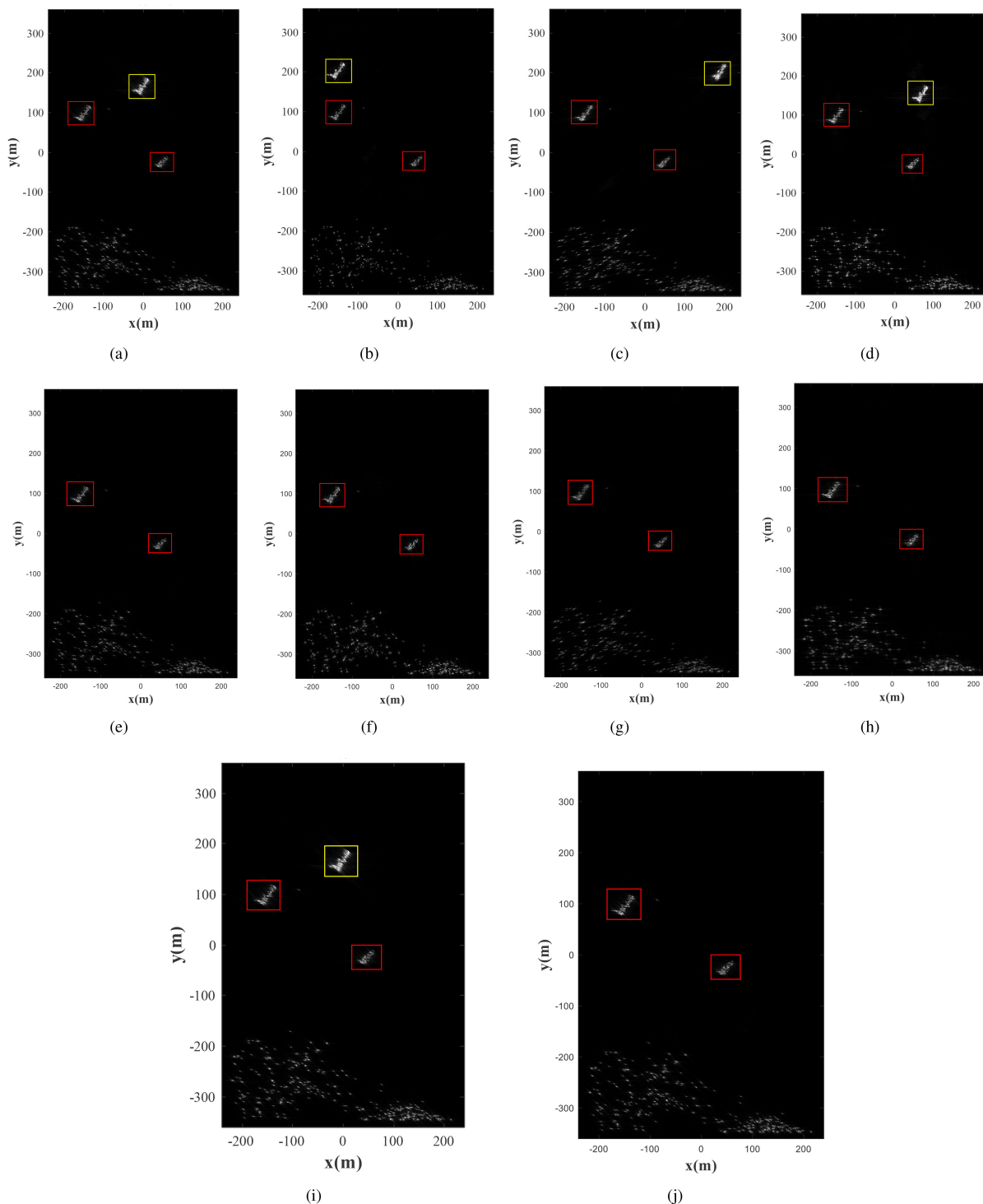
Fig. 6. Results of simulation experiment I. (a), (b), (c), and (d) are the images of receiver one, receiver two, receiver three and receiver four in the jamming environment. (e), (f), (g), and (h) are the images of receiver one, receiver two, receiver three and receiver four after beamforming. (i) and (j) are enlarged images of (a) and (e).

260, 20 m), and the fixed time delay is 0.7 μs. Fig. 7(a)–(d) is the images of the receiver one to the receiver four in the jamming environment. From the images, we can see that there is no difference between the strength of the real target and the false target, which will seriously affect the interpretation of the image.

If there is only one SAR image, we cannot distinguish which target is false. However, for multistatic SAR, we can detect and identify false targets. In four SAR images, we first analyze the relationship between targets, then use MSER algorithm and Euclidean-distance-based distinguish method to identify false
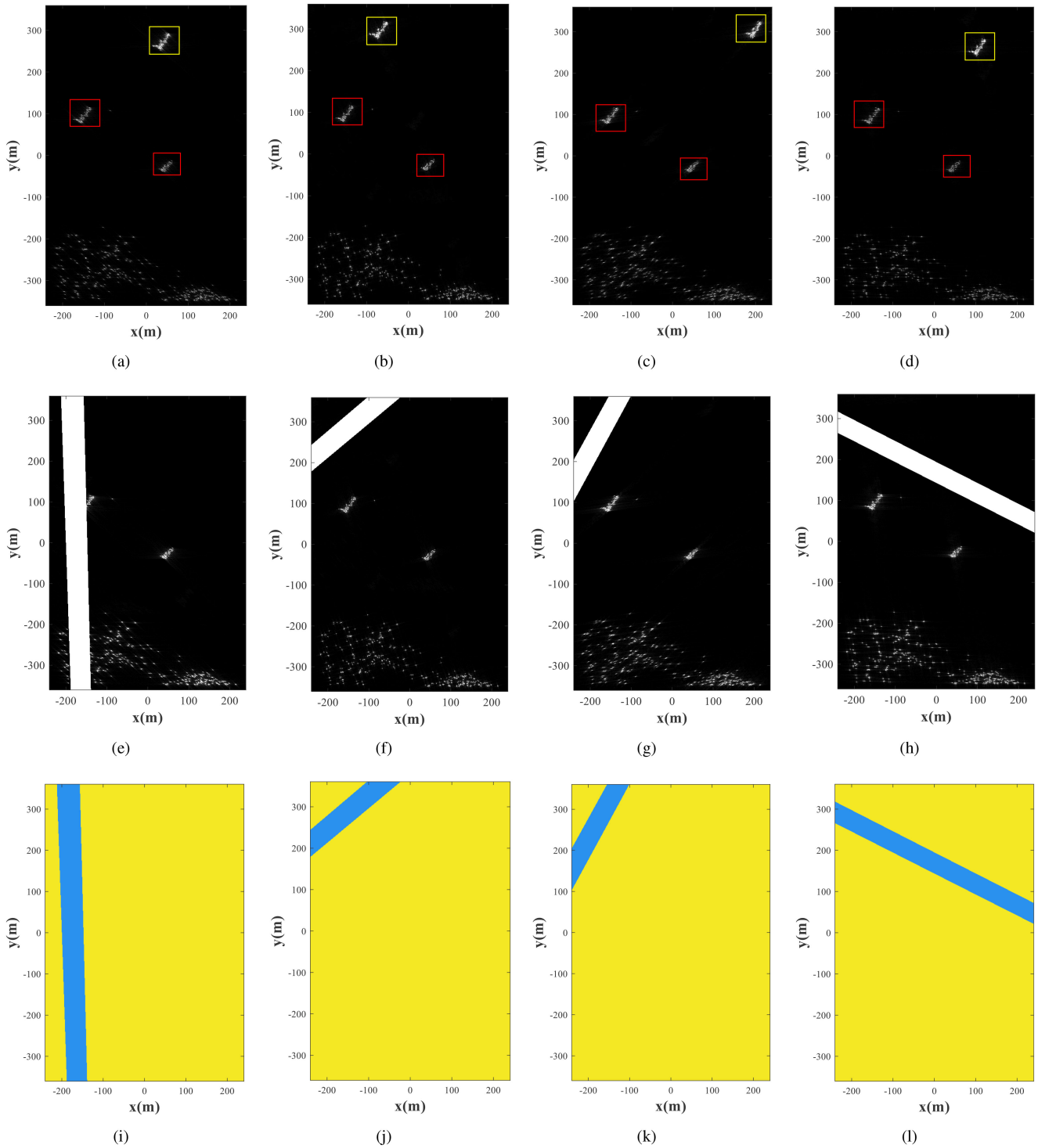
Fig. 7. Results of simulation experiment II. (a)–(d) Images of receiver one, receiver two, receiver three and receiver four under jamming environment. (e)–(h) Images of receiver one, receiver two, receiver three and receiver four after beamforming. (i)–(l) Effective imaging area of receiver one, receiver two, receiver three and receiver four.

targets in each image and obtain their location information. In images, the real targets are in the red rectangles, and the false targets are in the yellow rectangles.

Then, the MVDR algorithm nulls the direction of the receiver to the jammer. However, when the jammer is in the imaging area, if we directly use the MVDR algorithm to process the jamming signal, a blank area is appeared in each SAR image. The images after the MVDR algorithm are shown in Fig. 7(e)–(h), corresponding to receiver one to receiver four. The blank area in these four images is the blind area. Although false target no longer appears in the image, the imageable area is obviously reduced, and the information of the real target is also lost.
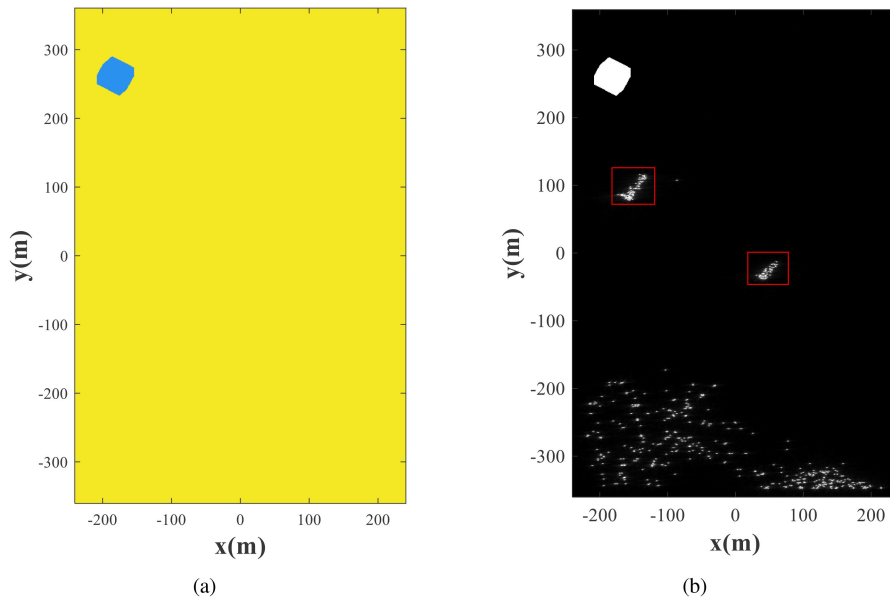
Fig. 8. Results of simulation experiment II after image mosaic method. (a) Effective imaging area after combining four receivers. (b) Final imaging results.

In order to enlarge the imageable area and avoid losing the real target information, the image mosaic method is apply to process the SAR image with blind area. Fig. 7(i)–(l) shows the effective imaging areas from receiver one to receiver four. In these images, the yellow area is the imageable area, and the blue area is the blind area. For each SAR image, we can see that the blind area occupies about 20% of the imaging area. That means that the image obtained by the four receivers has only 80% of the imageable area. Losing some of the real information will easily lead to our misjudgment of the image. For Bistatic SAR, this problem cannot be solved. In order to enlarge the imaging area, a new image mosaic method is proposed in this article. Fig. 8(a) shows the effective imaging area after overlapping Fig. 7 (i)–(l). In Fig. 8(a), in which the yellow area is the imageable area and the blue area is the blind area. Compared with the blue region in Fig. 7 (i)–(l), the blue region in the Fig. 8(a) is significantly reduced. This shows that the blind area is reduced by image mosaic method.

The yellow area is composed of multiple polygons, each representing a sub block. The selection method of each sub block is detailed in the above image mosaic method. Then, we synthesize a SAR image with good imaging performance and expandable imaging area by combining each optimal imaging sub block. The enlarged imaging area is the yellow area in Fig. 8(a). In this figure, we can see that there is still a small part of blue area, indicating that there is still a part of blind area in the image.

Fig. 8(b) shows the simulation image after eliminating the transmitting deceptive jamming by the above method, and the blank area is the blind area. In the image, we can see that the false target has been completely removed, and the imageable area has been significantly expanded.

The quantitative results for retransmitting deceptive jamming suppression for simulation experiment II are shown in Table III. The meaning of rows and columns are the same as Table II.

TABLE III
QUANTITATIVE RESULTS FOR RETRANSMITTING DECEPTIVE JAMMING
SUPPRESSION FOR SIMULATION EXPERIMENT II

$SIR_1{}^1$	$SIR_2{}^2$	SIR promotion
10	13.0443	3.0443
0	13.0440	13.0440
-10	13.0403	23.0403

[1] The SIR ratio before processing.
[2] The SIR ratio after processing.

From Table III, we can find that the suppression effect is not influenced by the power of jamming signal.

V. CONCLUSION

In this article, we propose a new multistatic SAR antideceptive jamming method, which can improve the effective interpretation of the image. Based on the model, we analyze the relationship among jammer, receiver, and transmitter, and derive the relationship between them. Next, the MSER detection algorithm is utilized to detect every target in the image. Then, the Euclidean-distance-based distinguish method is used to identify the false target in each SAR image and obtain the position information of the false target. By combining the above information, we can calculate the specific location of the jammer.

Based on the location of jammer, we mainly discuss the suppression effect of transmitting deceptive jamming in two situations. When the jammer is outside the imaging area, we can effectively remove the false target by using the MVDR algorithm, and it is not affect the imaging performance of the real target. For the other situation, the jammer is in the imaging area, the beamforming cannot directly and effectively remove

the false target without affecting the real target. When the MVDR algorithm is applied directly, a part of blind area is appeared in SAR image. In order to solve this problem, a new image mosaic method is proposed in this article. Taking advantage of the strengths of multistatic SAR system, we stitch and fuse the imaging information of multiple receivers, so as to effectively expand the imageable area. The simulation results have proved the effectiveness of the proposed method.

REFERENCES

[1] A. Moreira, P. Prats-Iraola, M. Younis, G. Krieger, I. Hajnsek, and K. P. Papathanassiou, "A tutorial on synthetic aperture radar," *IEEE Geosci. Remote Sens. Mag.*, vol. 1, no. 1, pp. 6–43, Mar. 2013.

[2] J. Wu, W. Pu, Y. Huang, J. Yang, and H. Yang, "Bistatic forward-looking SAR focusing using ω–k based on spectrum modeling and optimization," *IEEE J. Sel. Topics Appl. Earth Observ. Remote Sens.*, vol. 11, no. 11, pp. 4500–4512, Nov. 2018.

[3] W. Pu, Y. Huang, J. Wu, H. Yang, and J. Yang, "Fast compressive sensing-based SAR imaging integrated with motion compensation," *IEEE Access*, vol. 7, pp. 53 284–53 295, 2019.

[4] J. Wu, Z. Sun, H. An, J. Qu, and J. Yang, "Azimuth signal multichannel reconstruction and channel configuration design for geosynchronous spaceborneairborne bistatic SAR," *IEEE Trans. Geosci. Remote Sens.*, vol. 57, no. 4, pp. 1861–1872, Apr. 2019.

[5] J. Wu, Y. Li, W. Pu, Z. Li, and J. Yang, "An effective autofocus method for fast factorized back-projection," *IEEE Trans. Geosci. Remote Sens.*, vol. 57, no. 8, pp. 6145–6154, Aug. 2019.

[6] Z. Sun, J. Wu, J. Pei, Z. Li, Y. Huang, and J. Yang, "Inclined geosynchronous spaceborneairborne bistatic SAR: Performance analysis and mission design," *IEEE Trans. Geosci. Remote Sens.*, vol. 54, no. 1, pp. 343–357, Jan. 2016.

[7] M. Rodriguez-Cassola, P. Prats, G. Krieger, and A. Moreira, "Efficient time-domain image formation with precise topography accommodation for general bistatic SAR configurations," *IEEE Trans. Aerosp. Electron. Syst.*, vol. 47, no. 4, pp. 2949–2966, Oct. 2011.

[8] J. Bueso-Bello, M. Martone, P. Prats-Iraola, and B. Brutigam, "First characterization and performance evaluation of bistatic tanDEM-X experimental products," *IEEE J. Sel. Topics Appl. Earth Observ. Remote Sens.*, vol. 9, no. 3, pp. 1058–1071, Mar. 2016.

[9] F. Behner, S. Reuter, H. Nies, and O. Loffeld, "Synchronization and processing in the HITCHHIKER bistatic SAR experiment," *IEEE J. Sel. Topics Appl. Earth Observ. Remote Sens.*, vol. 9, no. 3, pp. 1028–1035, Mar. 2016.

[10] M. Rodriguez-Cassola, S. V. Baumgartner, G. Krieger, and A. Moreira, "Bistatic terraSAR-X/F-SAR spaceborneairborne SAR experiment: Description, data processing, and results," *IEEE Trans. Geosci. Remote Sens.*, vol. 48, no. 2, pp. 781–794, Feb. 2010.

[11] H. An, J. Wu, Z. Sun, and J. Yang, "A two-step nonlinear chirp scaling method for multichannel GEO spaceborne-airborne bistatic SAR spectrum reconstructing and focusing," *IEEE Trans. Geosci. Remote Sens.*, vol. 57, no. 6, pp. 3713–3728, Jun. 2019.

[12] V. Krishnan, J. Swoboda, C. E. Yarman, and B. Yazici, "Multistatic synthetic aperture radar image formation," *IEEE Trans. Image Process.*, vol. 19, no. 5, pp. 1290–1306, May 2010.

[13] M. Abbasi, A. Shayei, M. Shabany, and Z. Kavehvash, "Fast Fourier-based implementation of synthetic aperture radar algorithm for multistatic imaging system," *IEEE Trans. Instrum. Meas.*, vol. 68, no. 9, pp. 3339–3349, Sep. 2019.

[14] J. D. Coker and A. H. Tewfik, "Multistatic SAR image reconstruction based on an elliptical-geometry radon transform," in *Proc. Int. Waveform Diversity Des. Conf.*, Jun. 2007, pp. 204–208.

[15] H. An, J. Wu, Z. Sun, J. Yang, Y. Huang, and H. Yang, "Topology design for geosynchronous spaceborneairborne multistatic SAR," *IEEE Trans. Geosci. Remote Sens.*, vol. 15, no. 11, pp. 1715–1719, Nov. 2018.

[16] B. D. Rigling and R. L. Moses, "Three-dimensional surface reconstruction from multistatic SAR images," *IEEE Trans. Image Process.*, vol. 14, no. 8, pp. 1159–1171, Aug. 2005.

[17] D. Lloyd and I. D. Longstaff, "Ultra-wideband multistatic SAR for the detection and location of landmines," *IEEE. Proc. Radar Sonar Navigation*, vol. 150, no. 3, pp. 158–164, Jun. 2003.

[18] X. Chang and C. Dong, "A barrage noise jamming method based on double jammers against three channel SAR GMTI," *IEEE Access*, vol. 7, pp. 18755–18763, 2019.

[19] F. Liu and J. G. Wang, "Analysis of barrage-type jamming J/S isosurface to bistatic SAR," in *Proc. 2nd Asian Pac. Conf. Synthetic Aperture Radar*, 2010, pp. 18755–18763.

[20] W. Wang and J. Cai, "A technique for jamming bi- and multistatic SAR systems," *IEEE Geosci. Remote Sens. Lett.*, vol. 4, no. 1, pp. 80–82, Jan. 2007.

[21] Z. Bo, Z. Feng, and B. Zheng, "Deception jamming for squint SAR based on multiple receivers," *IEEE J. Sel. Topics Appl. Earth Observ. Remote Sens.*, vol. 8, no. 8, pp. 1–12, Aug. 2017.

[22] Z. Bo, H. Lei, Z. Feng, and J. Zhang, "Performance improvement of deception jamming against SAR based on minimum condition number," *IEEE J. Sel. Topics Appl. Earth Observ. Remote Sens.*, vol. 10, no. 3, pp. 1039–1055, Mar. 2017.

[23] X. Lin, P. Liu, and G. Xue, "Fast generation of SAR deceptive jamming signal based on inverse range Doppler algorithm," in *Proc. IET Int. Radar Conf.*, Apr. 2013, pp. 1–4.

[24] Z. Feng, Z. Bo, M. Tao, X. Bai, and G. Sun, "A large scene deceptive jamming method for space-borne SAR," *IEEE Trans. Geosci. Remote Sens.*, vol. 51, no. 8, pp. 4486–4495, Aug. 2013.

[25] Q. Sun, T. Shu, S. Zhou, B. Tang, and W. Yu, "A novel jamming signal generation method for deceptive SAR jammer," in *Proc. IEEE Radar Conf*, May 2014, pp. 1174–1178.

[26] B. Zhao, L. Huang, and J. Zhang, "Single channel SAR deception jamming suppression via dynamic aperture processing," *IEEE Sensors J.*, vol. 17, no. 13, pp. 4225–4230, Jul. 2017.

[27] L. Rosenberg and D. Gray, "Anti-jamming techniques for multichannel SAR imaging," *IEE Proc. Radar Sonar Navigation*, vol. 153, no. 3, pp. 234–242, Jun. 2006.

[28] R. Wang, B. Sun, C. Yi, J. Chen, and Y. Zhou, "Multi-channnel and MIMO SAR anti-jamming analysis," Jul. 2018, pp. 8006–8009.

[29] C. Li and D. Zhu, "The detection of deception jamming against SAR based on dual-aperture antenna cross-track interferometry," *J. Electron. Inf. Technol.*, 2007, pp. 1–4.

[30] Z. Wu, H. Xu, J. Li, and W. Liu, "Research of 3-D deceptive interfering method for single-pass spaceborne in SAR," in *IEEE Trans. Aerosp. Electron. Syst.*, vol. 51, no. 4, pp. 2834–2846, Oct. 2015.

[31] Q. Feng, H. Xu, Z. Wu, and W. Liu., "Deceptive jamming detection for SAR based on cross-track interferometry," in *Sensors.*, vol. 18, no. 7, 2018, Art. no. 2265.

[32] X. Qiu, T. Zhang, S. Li, T. Yuan, and F. Wang, "SAR anti-jamming technique using orthogonal LFM-PC hybrid modulated signal," in *Proc.China Int. SAR Symp.*, 2018, pp. 1–6.

[33] M. A. Hossain, I. Elshafiey, M. A. Alkanhal, and A. Mabrouk, "Anti-jamming capabilities of UWB-OFDM SAR," in *Proc. Eur. Radar Conf.*, Oct. 2011, pp. 313–316.

[34] W. Huo, Y. Huang, J. Pei, Q. Zhang, Q. Gu, and J. Yang, "Ship detection from ocean SAR image based on local contrast variance weighted information entropy," *Sensors*, vol. 18, no. 4, 2018, Art. no. 1196.

[35] J. Matas, O. Chum, M. Urban, and T. Pajdla, "Robust wide-baseline stereo from maximally stable extremal regions," *Image Vision Comput.*, vol. 22, no. 10, pp. 761–767.

[36] F. Jia, G. Sun, Z. He, and J. Li, "Grating-lobe clutter suppression in uniform subarray for airborne radar STAP," *IEEE Sensors J.*, vol. 19, no. 16, pp. 6956–6965, Aug. 2019.

[37] T. Bollian, B. Osmanoglu, R. Rincon, S.-K. Lee, and L. Fatoyinbo, "Adaptive antenna pattern notching of interference in synthetic aperture radar data using digital beamforming," *Remote. Sens.*, vol. 11, 2019, Art. no. 1346.

[38] M. Priyadarsini and C. Srinivasarao, "Beamforming in MIMO radar using coprime array," in *Proc. 2nd IEMENTech*, 2018, pp. 1–4.

[39] S. Hong, J. Li, Y. Ai, Y. Dong, Z. Zhao, and Y. Wang, "Bi-iterative MVDR beamforming based on beamspace preprocessing for MIMO radars," in *Proc. ISAPE*, 2018, pp. 1–4.

[40] J. Li, G. Liao, Y. Huang, J. Xu, Y. Xiang, and A. Nehorai, "MIMO-STAP based cognitive design of transmitted waveforms and receive filters for clutter suppression," in *Proc. IEEE Radar Conf*, 2018, pp. 1439–1444.

[41] J. Sanson, A. Gameiro, D. Castanheira, and P. P. Monteiro, "Comparison of DoA algorithms for MIMO OFDM radar," in *Proc. Eur. Radar Conf.*, 2018, pp. 226–229.

[42] R. G. Paxman and J. C. Marron, "Aberration correction of speckled imagery with an image-sharpness criterion," *Proc. SPIE Int. Soc. Opt. Photon.*, 1987, vol. 976, pp. 37–47.

[43] J. R. Fienup and J. J. Miller, "Aberration correction by maximizing generalized sharpness metrics," *J. Opt. Soc. Am.*, vol. 20, no. 4, pp. 609–620, 2003.

[44] R. A. Muller and A. Buffington, "Real-time correction of atmospherically degraded telescope images through image sharpening," *J. Opt. Soc. Am.*, vol. 64, pp. 1200–1210, 1974.

[45] J. N. Ash, "An autofocus method for backprojection imagery in synthetic aperture radar," *IEEE Geosci. Remote Sens. Lett.*, vol. 9, no. 1, pp. 104–108, Jan. 2012.

[46] S. Wei, X. Zhang, K. Hu, and W. Wu, "LASAR autofocus imaging using maximum sharpness back projection via semidefinite programming," in *Proc. IEEE Radar Conf. (RadarCon)*, May 2015, pp. 1311–1315.

[47] R. L. Morrison, M. N. Do, and D. C. Munson, "SAR image autofocus by sharpness optimization: A theoretical study," *IEEE Trans. Image Process.*, vol. 16, no. 9, pp. 2309–2321, Sep. 2007.

Jifang Pei (Member, IEEE) received the B.S. degree from the College of Information Engineering, Xiangtan University, Hunan, China, in 2010, the M.S. degree from the School of Electronic Engineering, University of Electronic Science and Technology of China, Chengdu, China, in 2013, and the Ph.D. degree from the School of Information and Communication Engineering, UESTC, in 2018.

From 2016 to 2017, he was a joint Ph.D. Student with the Department of Electrical and Computer Engineering, National University of Singapore, Singapore. He is currently an Associate Research Fellow with the School of Information and Communication Engineering, UESTC. His research interests include radar signal processing, machine learning, and automatic target recognition.

Wenjing Wang (Student Member, IEEE) received the B.S. degree from the School of Computer and Technology, China University of Mining and Technology, Xuzhou, China, in 2016.

She is currently working toward the Ph.D. degree with the University of Electronic Science and Technology of China, Chengdu, China.

Her research interests include synthetic aperture radar and signal processing.

Xinyu Mao received the B.S. degree in electronic engineering in 2019 from the University of Electronic Science and Technology of China, Chengdu, China, where she is currently working toward the M.S. degree.

Her research interests include synthetic aperture radar and airborne motion compensation.

Junjie Wu (Member, IEEE) received the B.S., M.S. and Ph.D. degrees in electronic engineering from the University of Electronic Science and Technology of China, Chengdu, China, in 2004, 2007, and 2013, respectively.

He is currently a Professor with the UESTC, Chengdu. From January 2012 to January 2013, he was a Visiting Student with the Department of Electrical and Computer Engineering, Duke University, USA. His research interests include synthetic aperture radar imaging (particular emphasis on bistatic synthetic aperture radar).

Mr. Wu is the reviewer of IEEE TGRS, TSP, JSTARS, JSTSP, GRS letters, IET RSN, etc.

Jianyu Yang (Member, IEEE) received the B.S. degree in electronic engineering from the National University of Defense Technology, Changsha, China, in 1984 and the M.S. and Ph.D. degrees in electronic engineering from the University of Electronic Science and Technology of China, Chengdu, China, in 1987 and 1991, respectively.

He is currently a Professor with the School of Electronic Engineering, UESTC. His research interests are mainly in synthetic aperture radar (SAR) and statistical signal processing.